Biochemical Pharmacology 81 (2011) 459–470

Contents lists available at ScienceDirect

Biochemical Pharmacology

journal homepage: www.elsevier.com/locate/biochempharm

Oxidative stress initiates DNA damager MNNG-induced poly(ADP-ribose)polymerase-1-dependent parthanatos cell death

Ling-Ya Chiu [a], Feng-Ming Ho [b], Shine-Gwo Shiah [c], Yung Chang [d], Wan-Wan Lin [a,*]

[a] Department of Pharmacology, College of Medicine, National Taiwan University, Taipei, Taiwan
[b] Department of Internal Medicine, Tao-Yuan General Hospital Department of Health, Executive Yuan, Taoyuan, Taiwan
[c] National Institute of Cancer Research, National Health Research Institutes, Zhunan, Miaoli County, Taiwan
[d] R&D Center for Membrane Technology and Department of Chemical Engineering, Chung Yuan Christian University, Taoyuan, Taiwan

ARTICLE INFO

Article history:
Received 26 August 2010
Accepted 27 October 2010

Keywords:
DNA damage
ROS
PARP-1
RIP1
JNK
Parthanatos

ABSTRACT

The alkylating agent N-methyl-N′-nitro-N′-nitrosoguanidine (MNNG) can cause excess DNA strand breaks that lead to poly(ADP-ribose)polymerase-1 (PARP-1) overactivation and cell death (parthanatos). However, the detail mechanism of MNNG-induced parthanatos was not well-investigated. In this study, we used MNNG-treated mouse embryonic fibroblasts (MEFs) to elucidate the signaling pathways of MNNG-induced parthanatos. We found that MNNG-induced cell death accompanied by rapid PARP-1 activation, c-Jun N-terminal kinase (JNK) activation, biphasic reactive oxygen species (ROS) production and intracellular calcium increase. The early ROS production occurring at 1 min and peaking at 5–15 min after MNNG treatment partially resulted from NADPH oxidase. In contrast, the late phase of ROS production occurring at 30 min and time-dependently increasing up to 6 h after MNNG treatment was generated by mitochondria. The antioxidant, NAC can abrogate all phenomena caused by MNNG. Results indicate that the calcium rise was downstream of early ROS production, and was involved in PARP-1 and JNK activation. Moreover, the PARP inhibitor was able to reduce MNNG-induced late-phase ROS production, calcium elevation, and cell death. Results further indicated the involvement of RIP1 in sustained ROS production and calcium increase. We characterized the interactive roles of ROS, calcium, JNK, and RIP1 in MNNG-induced cell death. We found that in addition to the alkylating property previously demonstrated, ROS production triggered by MNNG results in enhanced DNA damage and PARP-1 activation. Moreover, intracellular calcium elevation and ROS production have mutual amplification effects and thus contribute to PARP-1-mediated parthanatos.

1. Introduction

Poly(ADP-ribose) (PAR) polymerase-1 (PARP-1) is an abundant, chromatin-associated nuclear enzyme responsible for a unique post-translational polyADP-ribosylation reaction which is involved in DNA repair, transcriptional control, genomic stability, cell death and transformation [1,2]. Upon binding to DNA strand break sites, it uses NAD^+ as a substrate to synthesize long, branched PAR polymers to accept proteins responsible for DNA repair [1]. PARP-1 activation plays an essential role in DNA repair under moderate stress; however, in several pathological situations that involve massive DNA damage, extensive activation of PARP-1 can induce a specific form of cell death termed "parthanatos", which is morphologically characterized by membrane rupture, and condensed and shrunken nuclei [1,3].

The release of PARP activation-dependent apoptosis-inducing factor (AIF) from mitochondria, either directly through PAR targeting mitochondrial membranes [4] or indirectly through calpain activation [5], is a key player in parthanatos. Other than AIF release from mitochondria and translocation to the nucleus leading to nuclear condensation [4,5], excessive PARP-1 activation depletes cellular NAD^+ and its precursor, ATP, leading to irreversible cellular energy failure and mitochondrial dysfunction [2]. As to its pathophysiological importance, PARP-1-mediated cell death was implicated in several disease models, including ischemia-reperfusion injury after cerebral ischemia and myocardial infarction, inflammatory injury, reactive oxygen species (ROS)-induced injury, and glutamate-induced excitotoxicity [2,6,7].

Receptor interacting protein 1 (RIP1), a death domain containing serine/threonine kinase, was originally believed to be important for NF-κB activation [8,9]. Recently, increasing evidence showed that RIP1 plays an important role in mitochondria-dependent ROS generation, and the caspase-independent necrotic

* Corresponding author at: Rm. 1119, 11 Fl., 1 Ren-Ai Rd., Sec. 1, Zhongzheng Dist., Taipei City 100, Taiwan. Tel.: +886 2 23123456x88315; fax: +886 2 23513716.
E-mail addresses: wwllaura1119@ntu.edu.tw, wwl@ha.mc.ntu.edu.tw (W.-W. Lin).

0006-2952/$ – see front matter © 2010 Elsevier Inc. All rights reserved.
doi:10.1016/j.bcp.2010.10.016

cell death pathway [10–12]. In response to death insults, cytosolic RIP1 was demonstrated to be translocated to mitochondria where it can interrupt ANT-CypD interactions [13]. RIP1 was also reported to play an important role in PARP-1-mediated cell death. PARP-1 can activate c-Jun N-terminal kinase 1 (JNK1) through RIP1, and then JNK1 activation is required for AIF release. RIP1 deficiency or silencing of RIP1 can protect cells from PARP-1 hyperactivation-induced cell death [14].

Calcium has versatile biological functions and is an important messenger in many signaling pathways. Many genotoxic and PARP-activating stimuli, oxidative stress, and UV radiation can increase intracellular calcium levels, and thus the calcium signal contributes to cell death [15]. Calcium signals may be correlated with mitochondrial perturbations, because calcium chelators efficiently block the collapse of the mitochondrial membrane potential, secondary superoxide generation, and mitochondrial membrane damage [16]. Furthermore, calcium signals also play a role in the activation of PARP-1 [17–19].

Other than PAR complex accumulation and AIF translocation, more-detailed signaling pathways in parthanatos have not been identified. In particular, the roles of ROS, calcium, RIP1, and JNK in parthanatos-dependent cell death and their causal relationship to PARP-1 activation are not fully understood. Therefore, in this study, we used N-methyl-N′-nitro-N′-nitrosoguanidine (MNNG)-treated mouse embryonic fibroblasts (MEFs) as a cell model to clarify the death signals following PARP-1 activation. MNNG is an alkylating agent which has a nitrosourea structure and is a common tool for inducing PARP-1 activation. When treating MNNG at 0.5–10 μM, DNA damage is limited, and the physiological machinery, which normally plays homeostatic protective and regulatory roles, can repair the injury [20,21]. When DNA damage is extensive (e.g., MNNG treatment at 100–500 μM), cells cannot repair the injury. Then disproportionate activation of PARP-1 depletes the cellular pools of NAD^+ and ATP, resulting in cell death [14,20].

In this study, using specific molecule inhibitors we characterized the interactive roles of ROS, calcium, JNK, and RIP1 in MNNG-induced PARP-1 activation and cell death. We found that in addition to the alkylating property previously demonstrated, ROS production triggered by MNNG results in enhanced DNA damage and PARP-1 activation. Moreover, intracellular calcium elevation and ROS production have mutual amplification effects and thus contribute to PARP-1-mediated parthanatos.

2. Materials and methods

2.1. Materials

DMEM, RPMI 1640, FBS, penicillin and streptomycin were purchased from Gibco BRL (Grand Island, NY, USA). MNNG was obtained from Chem Service (West Chester, PA, USA). Polyclonal antibodies specific for β-actin, ERK2, p38, JNK1, and horseradish peroxidase-conjugated anti-mouse and anti-rabbit antibodies were purchased from Santa Cruz Biotechnology (Santa Cruz, CA, USA). Z-Val-Ala-Asp-fluoromethylketone (z-VAD-FMK), SB203580, SP600125, U0126 and BAPTA/AM were obtained from Calbiochem (San Diego, CA, USA). Phosphorylated antibodies of ERK, JNK, and p38 were purchased from Cell Signaling Technology (Beverly, MA, USA). Antibody against PAR was obtained from BD Pharmingen (San Diego, CA, USA). Butylated hydroxyanisol (BHA), N-acetylcysteine (NAC), diphenyliodonium (DPI), 2′,7′-dichloro-dihydrofluorescein diacetate ($DCFH_2$-DA), 3-(4,5-dimethylthiazol-2-yl)2,5-dephenyl-tetrazolium bromide (MTT), 3-aminobenzamide (3AB), 3,4-dihydro-5[4-(1-piperindinyl) butoxy]-1(2H)-isoquinoline (DPQ), rotenone and propidium iodide (PI) were obtained from Sigma–Aldrich (St. Louis, MO, USA). MitoSOX™ was purchased from Invitrogen-Molecular Probes (Eugene, OR, USA). CellTiter-Glo® Luminescent kit was purchased from Promega (Madison, WI, USA). 8-Hydroxy-2-deoxy guanosine (8-OH-dG) EIA kit was from Cayman Chemical (Ann Arbor, MI, USA). siRNA duplexes specific for mouse RIP1 (Catalog No. M-040150-00) were obtained from Dharmacon RNA Technologies (Lafayette, CO, USA). Nuclear Extraction Kit was purchased from Panomics (Santa Clara, CA, USA).

2.2. Cell culture

RIP1−/− MEFs were kindly provided by Dr. J. Han (Xiamen University, Fujian, China). Wild type and RIP1−/− MEFs as well as HeLa cervical cancer cells were cultured in DMEM, and HCT116 colon cancer cells were cultured in RPMI 1640, both supplemented with 10% (v/v) fetal bovine serum (FBS), 100 U/ml penicillin, 100 μg/ml streptomycin and incubated at 37 °C in a humidified atmosphere of 5% CO_2 in air.

2.3. Measurement of cell viability by MTT assay

Cells (10^4/ml) plated in 96-well plates were incubated with the indicated drugs at 37 °C. MTT (5 mg/ml) was added for 45 min, then the culture medium was removed, and the formazan granules generated by live cells were dissolved in 100% DMSO and shaken for 10 min. The optical densities (ODs) at 550 and 630 nm were measured using a microplate reader. The net absorbance (OD550–OD630) indicates the enzymatic activity of mitochondria and implies the cell viability.

2.4. Determination of ATP content

Cells (10^4/ml) plated in 96-well plates were treated with the indicated drugs at 37 °C. Cells were lysed, and the total intracellular ATP content was analyzed with the CellTiter-Glo® Luminescent kit following the manufacturer's instructions. Luminescence was measured in a Berthold LB96V MicroLumat plus (American Laboratory Trading, East Lyme, CT, USA). The ATP quantified in control cells was referred to as 100%.

2.5. Measurement of cell necrosis by propidium iodide (PI) uptake assay

Cell membrane integrity was assessed by determining the ability of cells to take up PI. Cells were trypsinized, collected by centrifugation, washed once with phosphate-buffered saline (PBS), and re-suspended in PBS containing 25 μg/ml of PI. The cells were incubated for 20 min at 37 °C. After incubation, cells were analyzed by FACScan flow cytometry (Becton Dickinson, Franklin Lakes, NJ, USA). The level of PI uptake by cells was quantified, and this represented the percentage of cell necrosis.

2.6. Immunoblot analysis

After stimulation, the medium was aspirated. Cells were rinsed twice with ice-cold PBS, and 25–100 μl of cell lysis buffer (20 mM Tris–HCl, pH 7.5, 125 mM NaCl, 1% Triton X-100, 1 mM $MgCl_2$, 25 mM β-glycerophosphate, 50 mM NaF, 100 μM Na_3VO_4, 1 mM PMSF, 10 μg/ml leupeptin, and 10 μg/ml aprotinin) was then added to each well. After harvesting, cell lysates were sonicated and centrifuged, and equal protein amounts of soluble protein, as determined by the Bradford protein assay, were denatured, subjected to sodium dodecylsulfate polyacrylamide gel electrophoresis (SDS-PAGE), and transferred to a polyvinylidene difluoride (PVDF) membrane. Nonspecific binding was blocked with TBST (50 mM Tris–HCl, pH 7.5, 150 mM NaCl, and 0.02% Tween 20) containing 5% nonfat milk for 1 h at room temperature. After immunoblotting with the first specific antibody, membranes were

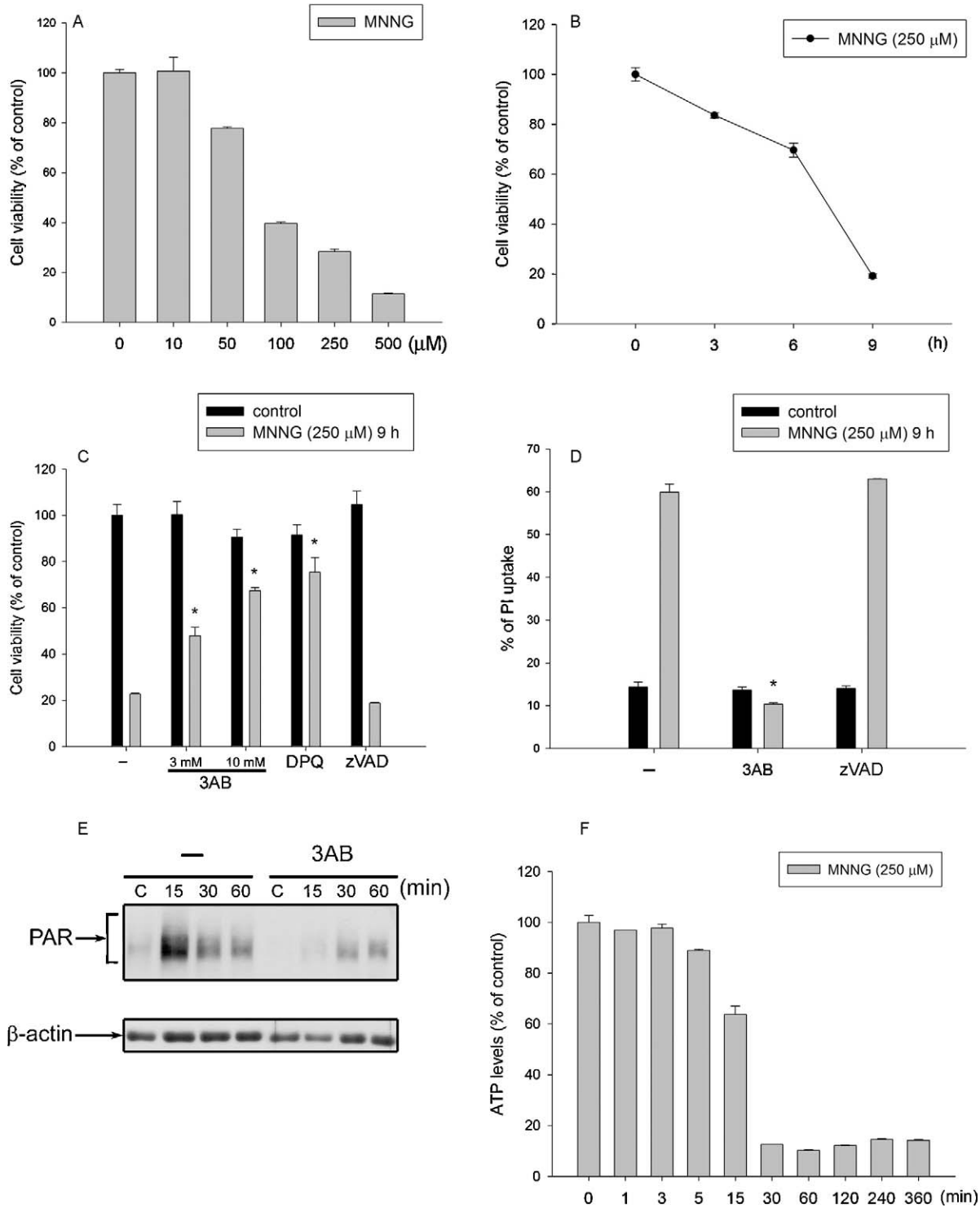

Fig. 1. MNNG-induced PARP activation leads to cell death in MEFs. (A) MEFs were treated with MNNG at the indicated concentrations for 9 h. Cell viability was assessed by an MTT assay. (B) MEFs were treated with MNNG (250 μM) for the indicated times. Cell viability was assessed by an MTT assay. (C) MEFs were pretreated with or without 3AB (3 or 10 mM), DPQ (50 μM) or zVAD (50 μM) for 30 min, then MNNG was added for 9 h. Cell viability was assessed by measuring the ATP content as described in Section 2. (D) MEFs were pretreated with or without 3AB (10 mM) or zVAD (50 μM), then MNNG was added for 9 h. Cells were harvested and incubated in PBS containing 25 μg/ml of PI. The percentage of PI uptake by dying cells was measured by FACScan. (E) MEFs were pretreated with or without 3AB (3 mM) for 30 min, and then MNNG (250 μM) was added for the indicated times. To determine the formation of PAR, total cell lysates were prepared and subjected to SDS-PAGE, followed by immunoblotting with a PAR antibody. β-Actin was used as the loading control. (F) MEFs were treated with MNNG (250 μM) for the indicated times. Intracellular ATP levels were assessed. Data are the mean ± S.E.M. from three independent experiments. $^{*}p < 0.05$, indicating the protective effects of 3AB on MNNG-induced responses.

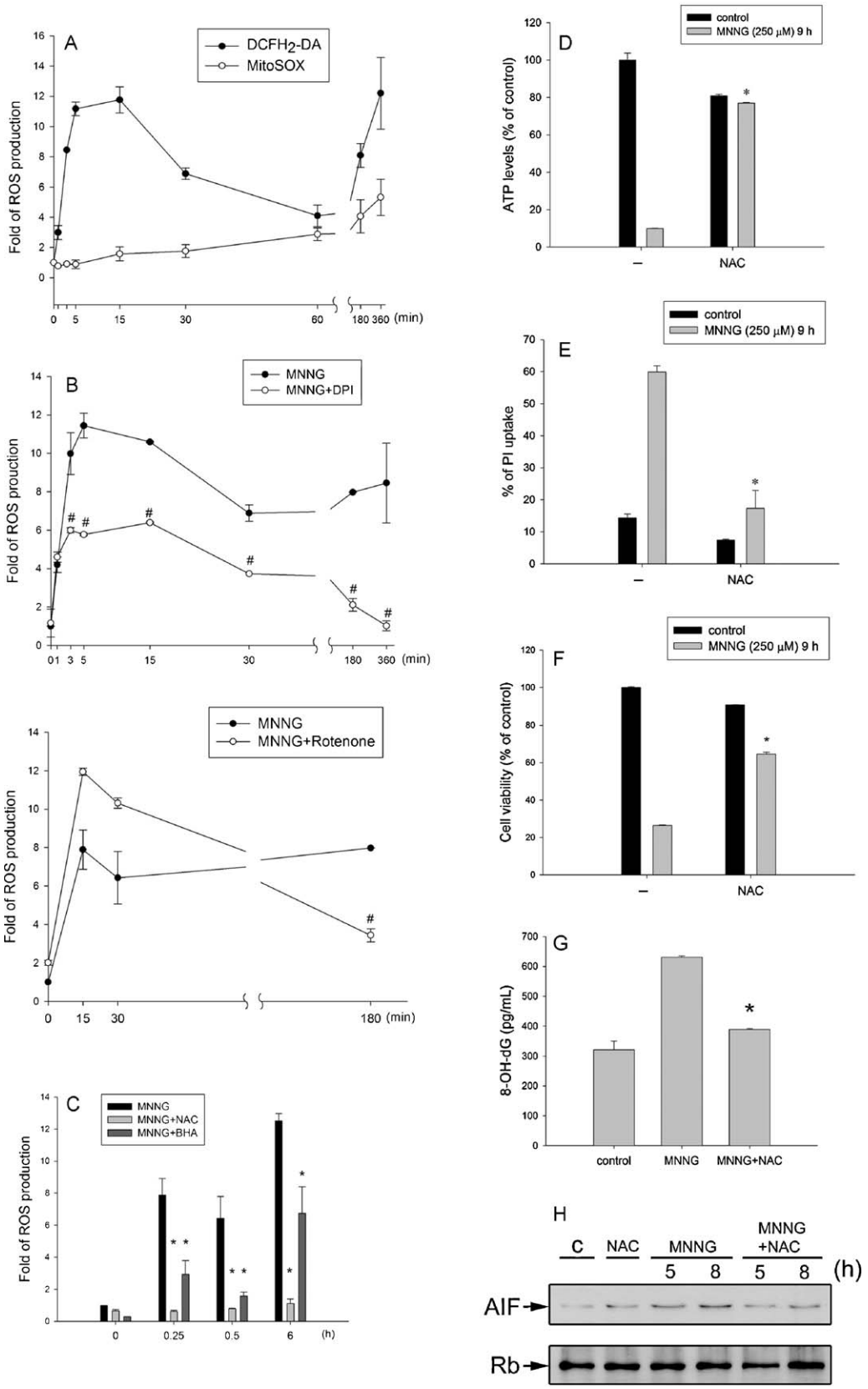

Fig. 2. ROS production is involved in MNNG-induced cell death. (A) MEFs were treated with MNNG (250 μM) for the indicated times. After treatment, cells were harvested, followed by measuring cytosolic and mitochondrial ROS as described in Section 2. (B) MEFs were pretreated with DPI (1 μM) or rotenone (1 μM) for 30 min, then MNNG (250 μM) was treated for the indicated times. After treatment, cells were harvested, followed by measurement of intracellular ROS. (C) MEFs were pretreated with NAC (10 mM) or BHA (150 μM) for 30 min, then MNNG (250 μM) was treated for the indicated times. After treatment, cells were harvested, followed by measurement of intracellular ROS. (D–F) MEFs were pretreated with NAC (10 mM) for 30 min, then MNNG (250 μM) was treated for 9 h, and intracellular ATP levels (D), PI uptake (E), and cell viability (F) were assessed. (G) MEFs were pretreated with or without NAC (10 mM) for 30 min, then MNNG (250 μM) was treated for 15 min. 8-Hydroxy-2-deoxy guanosine (8-OH-dG) levels were measured as described in Section 2. (H) MEFs were pretreated with or without NAC (10 mM) for 30 min, then MNNG (250 μM) was treated for the

washed three times with TBST and incubated with a horseradish peroxidase (HRP)-conjugated secondary antibody for 1 h. After three washes with TBST, the protein bands were detected with enhanced chemiluminescence detection reagent. To make sure equal amounts of sample protein were applied for electrophoresis and immunoblotting, β-actin was used as an internal control.

2.7. Cytosolic and mitochondrial ROS detection

To measure cytosolic ROS, we used $DCFH_2DA$, which can readily enter cells and be cleaved by esterase to yield DCFH, a polar, non-fluorescent product. ROS in cells promote the oxidation of DCFH to yield the fluorescent product, dichlorofluorescein. After treatment for the indicated time periods, cells were collected and then incubated in PBS containing the reagent $DCFH_2DA$ (5 μM) for 30 min at 37 °C. After incubation, cells were washed by PBS twice, trypsinized, re-suspended in 0.5 ml PBS, and immediately submitted to flow analysis using a FACScan flow cytometer. The data based on the FL1 channel were analyzed with the CellQuest program. To measure mitochondrial ROS, we used MitoSOX™, which is a live-cell permeant and is rapidly and selectively targeted to mitochondria. Once in the mitochondria, MitoSOX™ Red reagent is oxidized by superoxide and exhibits red fluorescence (with excitation at 510 nm and emission at 580 nm). After drug treatment for the indicated time periods, cells were collected and then incubated in Hank's balanced salt solution (HBSS) containing 5 μM MitoSOX™ for 30 min at 37 °C. After incubation, cells were washed with PBS twice, then trypsinized, re-suspended in 0.5 ml PBS, and immediately submitted to flow analysis. Data based on the FL2 channel were analyzed with the CellQuest program.

2.8. Nuclear fractionation

After treatment with MNNG or NAC, nuclear extracts were isolated using the Nuclear Extraction Kit according to the manufacturer's protocol. Briefly, 5×10^6 cells were washed with cold PBS twice. Buffer A (100 μl; 10 mM HEPES, pH 7.9, 10 mM KCl, 10 mM EDTA, 1 mM dithiothreitol, 0.4% [octylphenoxy] polyethoxyethanol, plus protease inhibitors) was added, and the plate was put on a rocking platform at 4 °C for 10 min. Cells were scraped from the plates, and cell clumps were disrupted by repetitive pipetting. The suspension was centrifuged at 15,000 × *g* at 4 °C for 5 min. The pellet was resuspended into 50 μl of buffer B (20 mM HEPES, pH 7.9, 200 mM NaCl, 1 mM EDTA, 10% glycerol, 1 mM dithiothreitol, plus protease inhibitors) by vigorous vortexing for 5 min and then at a medium vortex setting for 30 min at 4 °C. The suspension was centrifuged at 15,000 × *g* at 4 °C for 5 min, and the supernatant was collected (nuclear fraction). Equal amounts of protein extracts were subjected to immunoblot analysis and nuclear protein Rb was used as internal control.

2.9. Intracellular calcium ($[Ca^{2+}]_i$) measurement

Intracellular calcium was measured by Fluo-3. The most important properties of Fluo-3 are an absorption spectrum compatible with excitation at 488 nm by argon-ion laser sources, and a very large fluorescence intensity increase in response to Ca^{2+} binding. After treating cells with the indicated drugs for different time periods, cells were incubated in PBS containing Fluo-3 (3 μM) for 30 min at 37 °C. Cells were subjected to a flow analysis, and FL2 channel data were analyzed.

2.10. DNA damage measurement

We used a competitive enzyme-linked immunosorbent 8-OH-dG EIA kit to determine the 8-OH-dG levels of MEF cell lysates. Experimental procedures were performed as per the instructions in the manual.

2.11. Gene silencing with small interfering (si) RNA

The siRNA for RIP1 contained four RNA sequences in a SmartPool selected from the National Center for Biotechnology Information RefSeq Database using a proprietary algorithm. The control is a pool of four functional nontargeting siRNAs with guanine cytosine content comparable to that of the functional siRNA but lacking specificity for known gene targets. We transfected cells with the siRNA for 24–48 h, followed by drug treatment, and then evaluated the gene silencing effects by Western blot analysis.

2.12. Statistical evaluation

Values are expressed as the mean ± S.E.M. of at least three experiments. Analysis of variance was used to assess the statistical significance of the differences, with a p value of <0.05 considered statistically significant.

3. Results

3.1. MNNG induced parthanatos in MEFs

It was reported that the alkylating agent, MNNG, can produce DNA strands break and then activate PARP-1 leading to cell death. Herein, we confirmed the cell death effects induced by MNNG in MEFs. MNNG can induce cell death of MEFs in concentration- and time-dependent manners (Fig. 1A and B). This effect was inhibited by the PARP inhibitors, 3-aminobenzamide (3AB, 3 and 10 mM) and 3,4-dihydro-5[4-(1-piperindinyl) butoxy]-1(2H)-isoquinoline (DPQ, 50 μM), but not by zVAD (Fig. 1C), indicating that caspase activation might not participate in this pathway. Since a remarkable morphology of parthanatos is the rupture of plasma membranes, we conducted a PI uptake assay to verify whether cell integrity was destroyed with MNNG-induced cell death. We found that after 9 h of treatment, MNNG had largely increased PI uptake, and this effect was abrogated by PARP inhibitor (3AB) (10 mM). Again zVAD could not reverse this phenomenon (Fig. 1D). Immunoblot results indicated that MNNG could rapidly induce PAR formation, an index of PARP-1 activation, within 15 min. Moreover, MNNG-induced PAR formation was inhibited by 3AB (Fig. 1E). Then we evaluated the effect of MNNG on the intracellular ATP content. As shown in Fig. 1F, MNNG treatment significantly decreased the ATP level after 15 min of incubation and had almost completely depleted ATP after 30 min. The loss of ATP content lasted for at least 6 h, indicating that MNNG can induce rapid and long-lasting PARP-1 activation. Overall, MNNG could induce parthanatos in MEFs.

3.2. ROS is upstream of MNNG-induced parthanatos

To investigate whether ROS are involved in MNNG-induced parthanatos, we used the fluorescent dyes, $DCFH_2DA$ and MitoSOX, to respectively determine the cytosolic and mitochondrial ROS production after MNNG treatment. As shown in Fig. 2A, we found

indicated times. Nuclear fraction was prepared and equal amounts of nuclear protein were subjected to immunoblot analysis. Rb was used as internal control. Data are the mean ± S.E.M. from three independent experiments. $^{*}p < 0.05$, indicating the protective effects of NAC and BHA on MNNG-induced responses. $^{\#}p < 0.05$, indicating significant effects of DPI and rotenone on MNNG-induced ROS production.

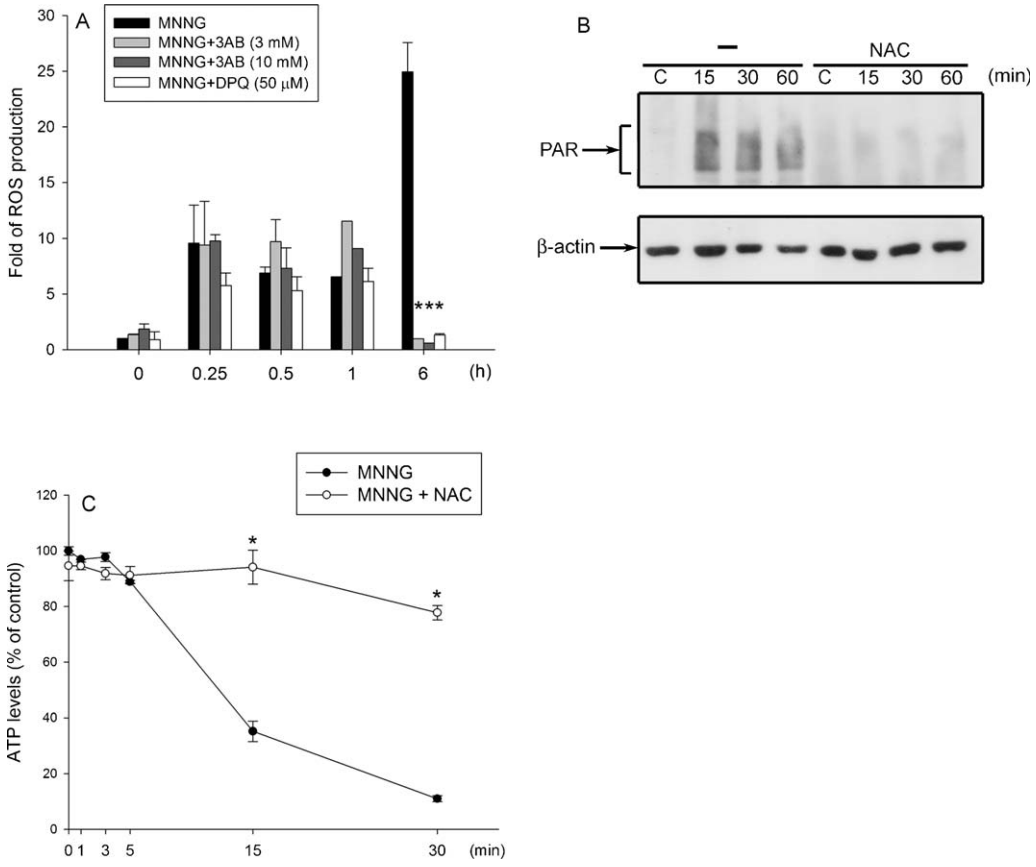

Fig. 3. Reciprocal interplay between MNNG-induced ROS production and PARP activation: early ROS production contributes to PARP activation. (A) MEFs were pretreated with 3AB (3 or 10 mM) or DPQ (50 μM), then MNNG (250 μM) was treated for indicated time periods. After treatment, cells were harvested, followed by cytosolic ROS measurement. (B) MEFs were pretreated with NAC (10 mM), and then MNNG (250 μM) was treated for the indicated time course. Total cell lysates were prepared and subjected to SDS-PAGE, followed by immunoblotting with a PAR antibody. β-Actin was used as a loading control. (C) MEFs were pretreated with or without NAC (10 mM), and then MNNG (250 μM) was treated for the indicated time periods. Intracellular ATP levels were measured and presented as the percentages of control cells. Data are the mean ± S.E.M. from three independent experiments. $^{*}p < 0.05$, indicating a significant inhibitory effect of 3AB and NAC on MNNG-induced responses.

that there was biphasic ROS production in the cytosol after MNNG treatment. The first phase appeared within 1 min and reached a peak within 5–15 min. The second phase gradually appeared from 1 to 6 h, the longest time point we tested. With mitochondrial ROS measurements, we found no significant ROS increase within 30 min of treatment with MNNG, but later mitochondrial ROS increased along with the incubation time up to 6 h. These results suggest that at least two different sources for ROS production are involved; the first phase which peaked at 5–15 min might not come from mitochondria, while the second phase that occurred after 30 min was derived from mitochondria.

Previous studies demonstrated that NADPH oxidase is responsible for tumor necrosis factor (TNF)-α-induced generation of O_2^- in mouse L929 fibrosarcomas [22], so we tested whether NADPH oxidase was the source of early-phase ROS production after MNNG treatment. Our results showed that the NADPH oxidase inhibitor, DPI (1 μM), was able to inhibit MNNG-elicited ROS production within 30 min by approximately 50%. DPI could also inhibit MNNG-induced ROS production for the longer time course of 3 and 6 h (Fig. 2B, upper panel). This phenomenon suggests that the first burst of ROS might be an important signal to initiate downstream events. We also used the mitochondrial complex 1 inhibitor, rotenone, to further verify whether the early phase of ROS comes from mitochondria. Results showed that rotenone did not inhibit, but even enhanced, the early phase of ROS production, ruling out a mitochondrial source for early ROS production. However, rotenone pretreatment inhibited ROS production in the late phase (3 h) (Fig. 2B, lower panel). Nevertheless both phases of ROS production were inhibited by the antioxidants, NAC and BHA (Fig. 2C). Moreover, NAC inhibited MNNG-induced ATP loss, PI uptake, and cytotoxicity (Fig. 2D–F). We also examined the 8-OH-dG level after MNNG treatment in MEFs, which represents oxidative stress-induced DNA strand breaks. NAC pretreatment reversed MNNG-induced 8-OH-dG elevation at 5 min of incubation (Fig. 2G). AIF translocation has been reported as a key player of parthanatos previously [1,4,23]. We also observed MNNG-induced AIF accumulation in the nuclear fraction. Otherwise, ROS scavenger can inhibit AIF translocation (Fig. 2H). Overall, ROS production participates in MNNG-induced parthanatos, and NADPH oxidase might contribute to the early phase of ROS production.

After showing the contribution of PARP and ROS in MNNG-induced parthanatos, we wanted to investigate in detail the causal relationship between both events. First, we used the PARP inhibitors, 3AB and DPQ, to examine their effects on ROS production. As shown in Fig. 3A, 3AB and DPQ effectively inhibited the late phase of ROS production at 6 h, but could not inhibit the early phase. Moreover, NAC pretreatment not only inhibited MNNG-induced PAR formation within 1 h (Fig. 3B), but also maintained the ATP level following MNNG treatment (Fig. 3C). These results suggest that MNNG-induced rapid ROS production is upstream of PARP-1 activation, while the latter response is also involved in amplification of the ROS increase.

3.3. MNNG-induced ROS mediates mitogen-activated protein kinases (MAPKs) activation, and JNK amplifies ROS production

MAPKs are important signaling cascades involved in regulating cell death, so we investigated their roles in MNNG-induced

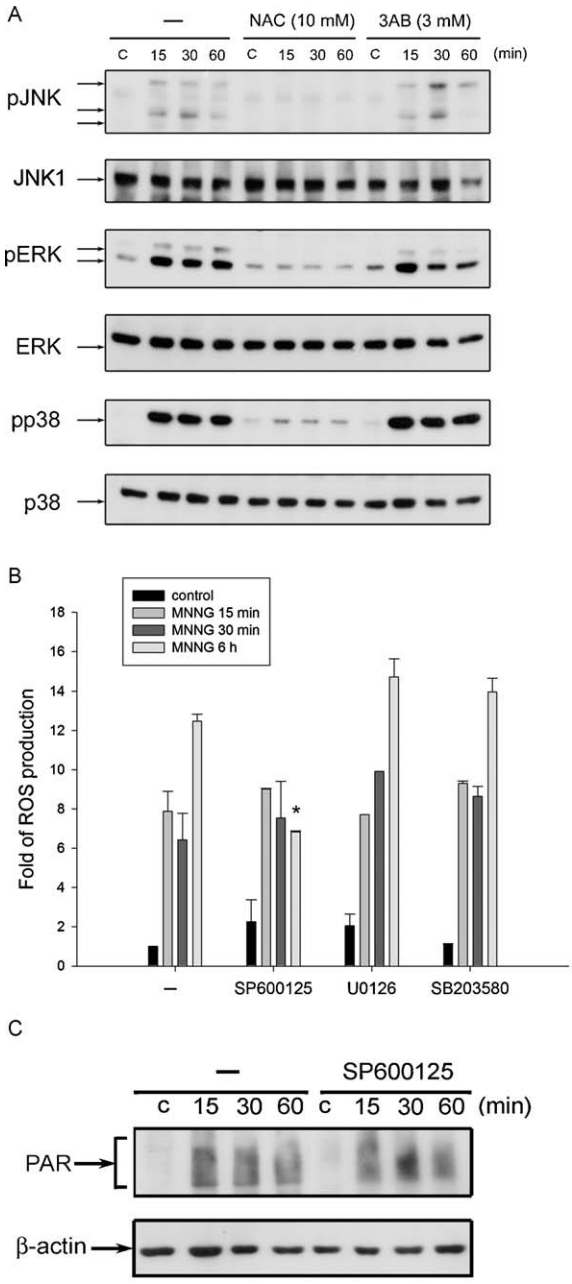

Fig. 4. Positive interaction between ROS production and JNK activation. (A) MEFs were pretreated with or without NAC (10 mM) and 3AB (10 mM), and then MNNG was treated for the indicated time periods. To determine the phosphorylation status of MAPKs, total cell lysates were prepared and subjected to SDS-PAGE, followed by immunoblotting with phosphorylated JNK, ERK, and p38 antibodies. Total levels of JNK1, ERK, and p38 were used as the loading controls. (B) MEFs were pretreated with SP600125 (10 μM), U0126 (10 μM), or SB203580 (10 μM) for 30 min, and then treated with MNNG (250 μM) for the indicated time periods. After treatment, cells were harvested, followed by measurement of intracellular ROS. Data are the mean ± S.E.M. from three independent experiments. $^{*}p < 0.05$, indicating the significant inhibition of MNNG response by SP600125. (C) MEFs were pretreated with SP600125 (10 μM), and then MNNG was treated for the indicated time course. Total cell lysates were prepared and subjected to SDS-PAGE, followed by immunoblotting with a PAR antibody. β-Actin was used as a loading control.

parthanatos. We found that MNNG could strongly induce extracellular signal-regulated kinase (ERK), JNK, and p38 phosphorylation within 1 h, but after pretreatment with NAC, MAPKs activation was significantly inhibited. In contrast, 3AB pretreatment did not inhibit MNNG-induced MAPKs activation (Fig. 4A). These data demonstrate that MAPKs, but not PARP-1, activation is mediated by the early phase of ROS production. Next, we used SP600125 (a JNK inhibitor), U0126 (a MEK inhibitor), and SB203580 (a p38 inhibitor) pretreatment to elucidate the relationship between the early and late phases of ROS production and MAPKs activation. We found that only the JNK inhibitor, SP600125, could inhibit the late phase but not the early phase of ROS production. The other two inhibitors exhibited no inhibition on either the early or late phase of ROS production (Fig. 4B). Moreover, to elucidate consequences of JNK and PARP, we treated cells with SP600125 before determining PAR formation. As a result, we found that SP600125 pretreatment did not affect MNNG-induced PAR formation (Fig. 4C). These results together with above ones indicate that MNNG-induced early ROS production mediates MAPKs and PARP activation. In turn, JNK further amplifies sustained ROS production.

3.4. An increase in calcium is involved in the MNNG-induced signaling pathway

Since calcium is a crucial signal in the cell death pathway, we tested whether cytosolic calcium levels changed after MNNG treatment. As shown in Fig. 5A, MNNG increased intracellular calcium levels in MEFs after 15 min of incubation, and this increasing effect continued until 6 h. Since ROS production and PARP-1 activation also occurred within 15 min, we investigated the regulation among ROS, PARP-1, and calcium. As a result, NAC pretreatment significantly inhibited the calcium increase in both the early or late time courses (Fig. 5A). Even though 3AB significantly inhibited the calcium increase after 30 min, but not at 15 min (Fig. 5A), chelating intracellular calcium with BAPTA/AM decreased PAR formation within 1 h (Fig. 5B). These results suggest that an ROS-dependent calcium increase is required for PARP activation. To understand if calcium is involved in ROS-dependent JNK signaling as we mentioned above, we determined the effect of BAPTA/AM. Results further showed that BAPTA/AM inhibited MNNG-induced JNK activation (Fig. 5B). Moreover, BAPTA/AM did not alter the early phase of ROS production, but inhibited the late-phase response (Fig. 5C). In agreement with this finding, BAPTA/AM could partially protect MEFs against MNNG-induced cell death as assessed by the attenuation of ATP loss upon MNNG treatment from 15 min to 9 h (Fig. 5D). These data indicate that the early phase of ROS production is upstream of the calcium increase within 15 min, which independently leads to PARP-1 and JNK activation, followed by triggering sustained increases in ROS and calcium.

3.5. RIP1 is required for the MNNG-induced late phase of ROS production, calcium elevation, and cell death

Previous reports demonstrated that MNNG-induced cell death is RIP1-dependent [14]. To understand the role of RIP1 in parthanatos signaling mediated by MNNG, we tested the effects of MNNG in RIP1−/− MEFs. We found that MNNG-induced cell death was attenuated, but not abrogated, in RIP1-deficient MEFs (Fig. 6A). Knocking down RIP1 with specific siRNA can also obtain the similar result (Fig. 6F, upper panel). Next we examined the ROS production and calcium increase in RIP1−/− MEFs. Results revealed that only the late phase, not the early phase, of ROS production was inhibited in RIP1−/− MEFs and also RIP1 silencing cells (Fig. 6B and F, lower panel). Consistently, MNNG still induced comparable calcium increases in wild-type (WT) and RIP1−/− cells within 3 h, but the late phase of calcium increase at 6 h was reduced by a deficiency of RIP1 (Fig. 6C). When testing intracellular ATP levels, we found that RIP1−/− MEFs had a similar susceptibility as did WT cells for early ATP depletion in response to MNNG treatment. However, the sustained ATP depletion within 3–9 h was

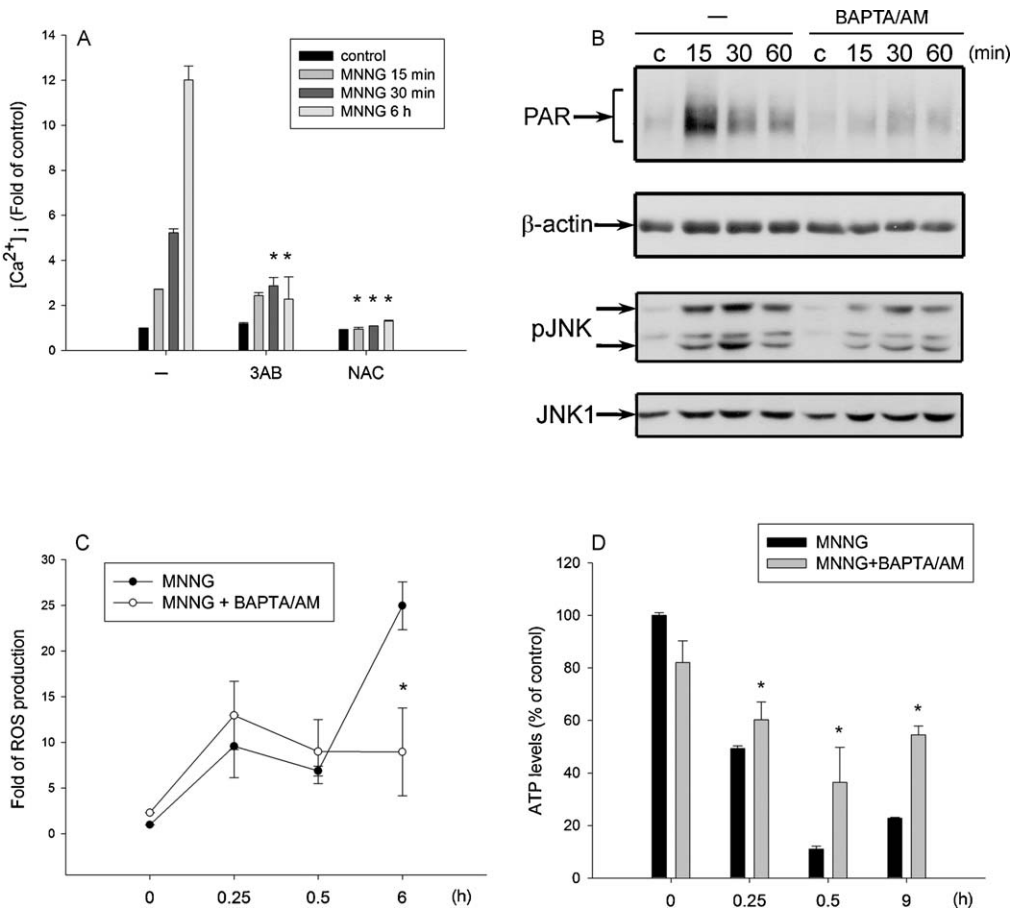

Fig. 5. Intracellular calcium increase is upstream of PARP activation and reciprocally interacts with ROS. (A) MEFs were pretreated with the vehicle, 3AB (10 mM), or NAC (10 mM) for 30 min, then treated with MNNG (250 μM) for the indicated time periods. After treatment, cells were harvested, followed by measurement of intracellular calcium as described in Section 2. (B) MEFs were pretreated with or without BAPTA/AM (10 μM), and then MNNG (250 μM) was added for the time indicated. Total cell lysates were prepared and subjected to SDS-PAGE, followed by immunoblotting with PAR, phosphorylated JNK, and JNK1. β-Actin was used as a loading control. (C) MEFs were pretreated with BAPTA/AM (10 μM), then MNNG (250 μM) was treated. After treatment for different periods, cells were harvested, followed by measurement of intracellular ROS. (D) MEFs were pretreated with BAPTA/AM (10 μM) for 30 min, and then MNNG (250 μM) was treated for the indicated time intervals. Cell viability was assessed by the ATP content. Data are the mean ± S.E.M. from three independent experiments. $^{*}p < 0.05$, indicating significant inhibition of MNNG responses by 3AB, NAC, and BAPTA/AM.

partially inhibited in RIP1−/− MEFs (Fig. 6D). Consistent with the non-effectiveness of RIP1 deficiency on the early death mediators (ROS, calcium, and ATP loss), we found that MNNG-induced PARP-1 and JNK activations within 1 h were not significantly altered in RIP1−/− cells compared to control WT cells (Fig. 6E). These results suggest that RIP1 might not participate in the regulation of early PARP-1 activation but is required for sustained ROS production, calcium increase, and ATP loss in response to MNNG.

3.6. MNNG also induced oxidative stress and parthanatos in cancer cells

We wonder whether MNNG-induced parthanotos is a general effect among different cell types. As shown in Fig. 7A, MNNG can also induce significant cell death in HeLa and HCT116 cancer cells after 9 h incubation. However, cancer cells were more sensitive to lower dose (50 μM) of MNNG as compared to MEFs (Fig. 1A). We also found that MNNG as its effect observed in MEFs can induce ROS production either at early phase (15 min) or at late phase (6 h) in both cancer cell types (Fig. 7B). Results revealed that higher fold of ROS production was induced by MNNG in HeLa cells than in HCT116 cells. In addition, there were also rapid PAR complex formation and JNK activation after MNNG treatment in both cancer cell types (Fig. 7C).

4. Discussion

PARP-1 activation was shown to play important roles in the pathogenesis of many diseases and tissue injuries, such as ischemia-reperfusion injury after cerebral ischemia and myocardial infarction, inflammatory injury, ROS-induced injury, and glutamate excitotoxicity [2,5,14,24]. In this study, in an attempt to elucidate the regulating mechanisms for PARP-1 activation, MNNG was used as a PARP-1 activator. As reported, MNNG is a nitrosourea compound which is used as an alkylating agent. These compounds covalently modify bases in the DNA, resulting in massive production of DNA strand breaks; PARP-1 is then activated to repair the damage. To understand the molecular details of PARP-1-dependent cell death, we used MNNG and confirmed its effect in inducing PARP-1 hyperactivation, as represented by the formation of PAR (Fig. 1E), the decrease in ATP content (Fig. 1F), and MEF cell death (Fig. 1A and B). Moreover, consistent with previous reports [15], we found that the PARP inhibitors, 3AB and DPQ, could protect cells against cell death (Fig. 1C and D), indicating that PARP-1 mediates MNNG-induced cell death in MEFs.

Intriguingly, our results showed that MNNG could rapidly induce ROS production within 1–15 min when stained with $DCFH_2$-DA but not with MitoSOX. But after incubation for 0.5–6 h, $DCFH_2$-DA detected another peak production of ROS, and MitoSOX also detected the increase in ROS (Fig. 2A). These results

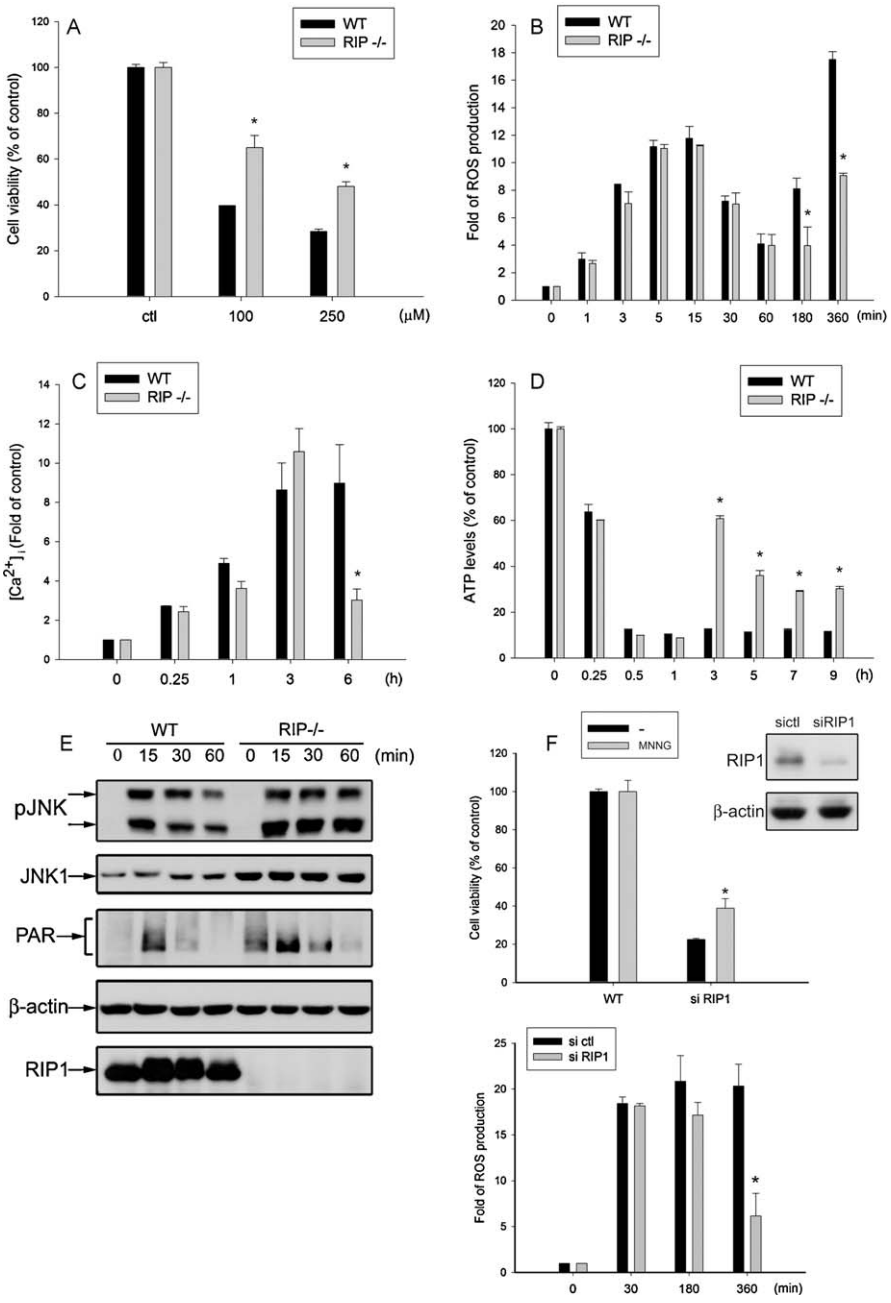

Fig. 6. RIP1 is required for MNNG-induced ROS production and cell death. (A) Wild type (WT) and RIP1−/− MEFs were treated with MNNG at the indicated concentrations for 9 h. Cell viability was assessed by an MTT assay. (B) WT and RIP1−/− MEFs were treated with MNNG (250 μM) for different intervals. After treatment, cells were harvested, followed by measurement of intracellular ROS. (C) WT and RIP1−/− MEFs were pretreated with MNNG (250 μM) for the indicated time intervals. After treatment, cells were harvested, followed by measurement of intracellular calcium. (D) WT and RIP1−/− MEFs were treated with MNNG (250 μM) for the indicated time, and then the intracellular ATP level was determined. Data are the mean ± S.E.M. from three independent experiments. (E) WT and RIP1−/− MEFs were treated with MNNG (250 μM) for the indicated time. Total cell lysates were prepared and subjected to SDS-PAGE, followed by immunoblotting with PAR and phosphorylated JNK. β-Actin and JNK1 were used as the loading controls. (F) Wild-type MEFs were transfected with RIP1 siRNA to knock down endogenous RIP1 or with non-targeting siRNA as a control. After transfection for 48 h, cells were treated with MNNG (250 μM), then cell viability at 9 h (upper panel) and intracellular ROS production at indicated time (lower panel) were determined by MTT assay and flow cytometry, respectively. RIP1 protein expression was determined by immunoblot. $^{*}p < 0.05$, indicating significant inhibition of MNNG-induced responses in RIP1−/− or RIP1 silencing cells.

together with the inhibitory effect of rotenone on late-phase ROS production (Fig. 2B) indicate that there is a biphasic ROS production in MEFs following MNNG treatment, and the late phase of ROS production might be generated from mitochondria. These findings support a previous notion that mitochondrial dysfunction is involved in MNNG-induced cell death [4,25]. Our data ruled out the origin of the first phase of ROS production being from mitochondria. Since DPI significantly inhibited the early ROS production (Fig. 2B), NADPH oxidase might be the source for early phase ROS production.

In addition to activating PARP-1 via alkylating agent-induced DNA strand breaks as previously described, our results notably showed that oxidative stress is crucial for MNNG to induce PARP-1 activation. In our study, PARP inhibitors (3AB and DPQ) did not inhibit the early phase of ROS production (Fig. 3A), while NAC effectively abolished PARP-1 activation (Fig. 3B). We also compared the time course of the early-phase ROS production and PARP-1 activation. We found that the timing of ROS production was earlier than that of ATP depletion, suggesting that the early-phase ROS increase might be an upstream signal for PARP-1

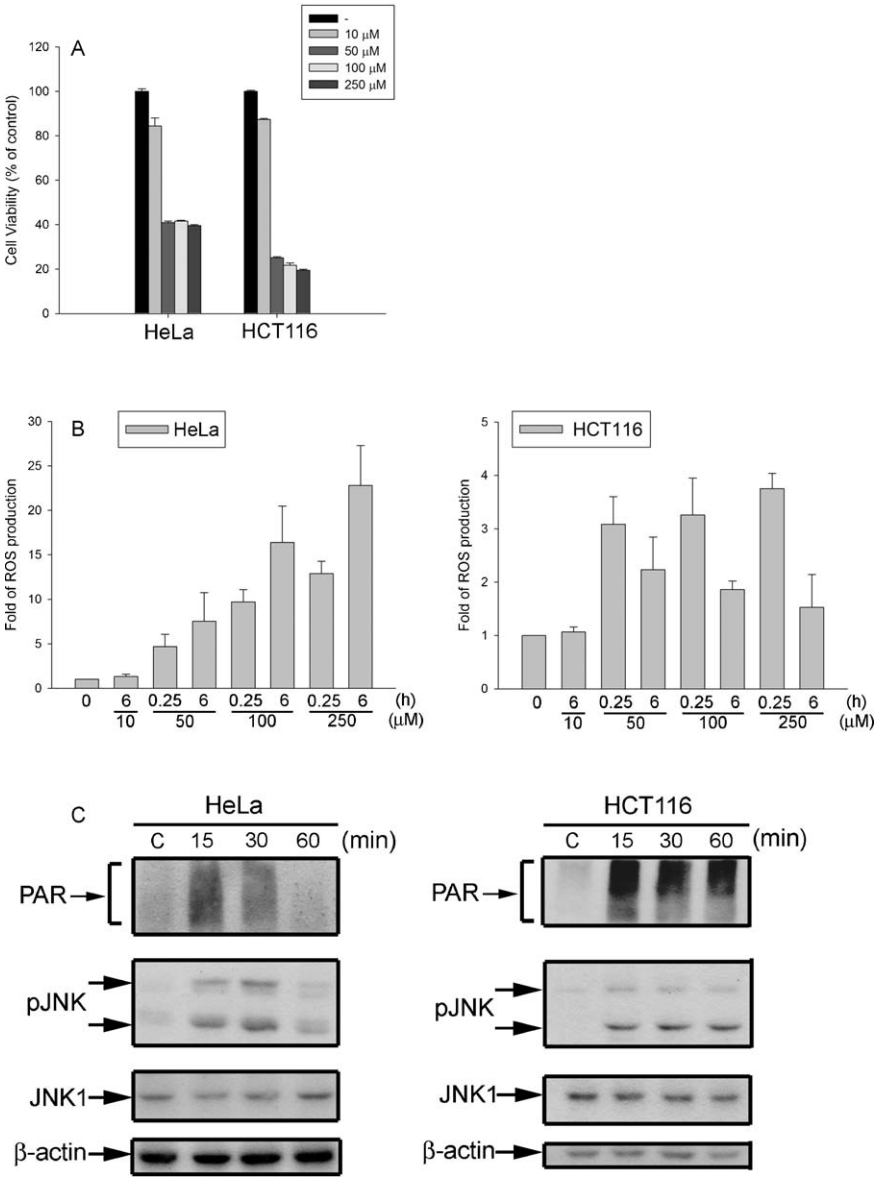

Fig. 7. MNNG also induced oxidative stress and parthanatos in cancer cells. (A) HeLa and HCT116 were treated with MNNG at the indicated concentrations for 9 h. Cell viability was assessed by an MTT assay. (B) HeLa and HCT116 were treated with MNNG at the indicated concentration for the indicated time periods. After treatment, cells were harvested, followed by measuring cytosolic ROS. Data are the mean ± S.E.M. from three independent experiments. (C) HeLa and HCT116 were treated with MNNG (100 μM) for the time indicated. Total cell lysates were prepared and subjected to SDS-PAGE, followed by immunoblotting with PAR, and JNK. β-Actin was used as a loading control.

activation. Even though our present data cannot rule out the contribution of direct DNA alkylation in MNNG-induced DNA damage and PARP-1 activation, we suggest rapid and marked ROS increase rather than DNA alkylation might plays a major role in MNNG-induced PAPR-1 activation. This suggestion is based on the abolishment of rapid PAR formation by NAC as well as BAPTA/AM (see below). Consistently, previous findings also demonstrated that oxidative stress can activate PARP-1 and trigger downstream signaling [26–28].

ROS are important second messengers in many signaling pathways, and activate many downstream kinases to transduce signals. We found that MNNG treatment significantly induced MAPK activation, and this event was mediated by early-phase ROS production (Fig. 4A). Nevertheless, neither SP600125 (a JNK inhibitor), U0126 (a MEK inhibitor), nor SB203580 (a p38 inhibitor) inhibited early-phase ROS production (Fig. 4B). A previous study reported that PARP-1 can activate JNK1 through the RIP1 and TRAF2 complex, and JNK1 activation is required for AIF release, indicating the importance of JNK1 in PARP-1-mediated necrosis [14]. In our results, we found that JNK might participate in the late-phase ROS production, since SP600125 did not influence the early-phase but did inhibit the late-phase ROS increase (Fig. 4B). Thus the interconnectivity and amplification network between ROS and JNK, which was extensively documented [29–32], was also suggested in the case of MNNG.

In this study, we found that MNNG induced a Ca^{2+} level increase after 15 min which was sustained to 6 h (Fig. 5A). We also showed that the early-phase ROS increase might be the upstream signal of the Ca^{2+} increase (Fig. 5A), and Ca^{2+} may in turn regulate PARP-1 activation (Fig. 5B and D). This finding is consistent with previous studies suggesting that Ca^{2+} is an important co-factor for PARP-1 hyperactivation either in the absence (e.g., electrical stimulation) or presence of DNA breaks (e.g., after ROS-induced DNA damage) [17,19]. Other than the regulatory role for PARP-1 activation in the early stage, we also found that the Ca^{2+} signal is involved in regulating late-phase ROS production. Since BAPTA/AM can inhibit

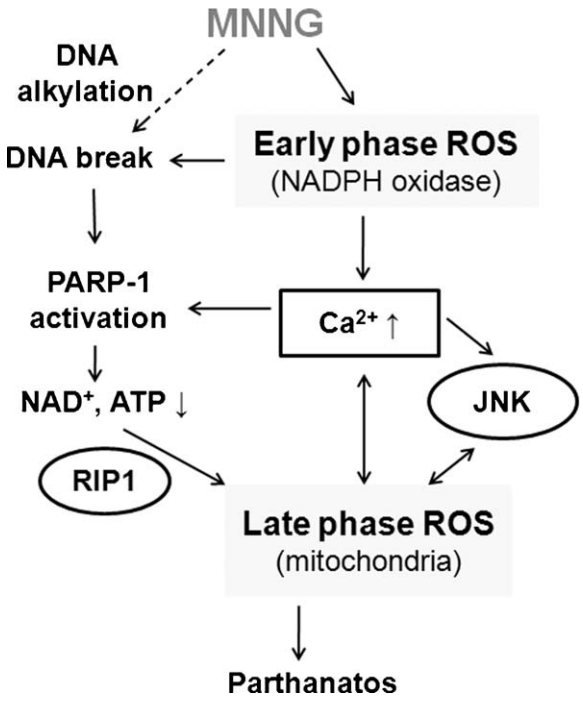

Fig. 8. Summary of the signaling pathways for MNNG-induced cell death.

late-phase ROS (Fig. 5C), and NAC can also abrogate Ca^{2+} rise at 6 h (Fig. 5A), there may be a loop amplification between the late phase of ROS production and the Ca^{2+} increase.

Previous reports demonstrated that PARP-1 activation leads to JNK1 activation and a subsequent cell death program through RIP1/TRAF2 [14]. In this study, based on the result that MNNG-induced cell death was more resistant in RIP1 knockout or silencing cells than WT cells (Fig. 6A and F), we also confirmed the involvement of RIP1 in MNNG-induced parthanatos. However, in our study, since MNNG-induced JNK activation with a 60-min incubation was not reversed by PARP-1 inhibition (Fig. 4A), and this action showed no significant difference between WT and RIP1−/− MEFs (Fig. 6E), we suggest that JNK activation is independent of PARP-1 and RIP1 activation. Nevertheless, from our results shown in Figs. 4B, 6B and F, JNK and RIP1 may both participate in regulating the late-phase ROS event.

Currently, molecular mechanisms for RIP1-dependent ROS production are well documented. RIP1 was shown to inhibit ANT-conducted ADP transport into mitochondria, leading to a progressive reduction in ATP levels, vacuolization of organelles, and disintegration of plasma membranes, with only negligible nuclear shrinkage [22]. Inhibition of ADP/ATP exchange coincides with sustained H_2O_2 production, so RIP1 may have an important regulatory role in mitochondrial ROS production [13]. Since MNNG-induced late-phase ROS also came from mitochondria, we suggest that RIP1-elicited mitochondrial dysfunction contributes to parthanatos. Recently, some papers discussed the importance of RIP3, a protein kinase that has an N-terminal kinase domain similar to that found in RIP1. Studies revealed that RIP3 may participate in regulating the switch between apoptosis and necrosis after TNF-α treatment [33]. RIP3 can interact with some key metabolic enzymes during necrosis, like glycogen phosphorylase, glutamate-ammonia ligase, and glutamate dehydrogenase, and might thus increase energy metabolism-associated ROS production [33]. In MNNG-induced parthanatos, besides involving in late-phase ROS production and energy loss (Fig. 6B, D and F), whether RIP1 shares similar mechanistic action in metabolic enzymes as RIP3 does in promoting necrosis is an intriguing topic for further investigation.

It was interesting to note that compared to the protective extents exerted by a PARP inhibitor and ROS scavenger, RIP1 deficiency only moderately prevented cell death (Fig. 6A and F). In light of this finding, we propose that besides acting as a death mediator, RIP1 might also be involved in other signals induced by DNA strand breaks. In this aspect, recent studies indicated that RIP1 is critical for NF-κB activation during DNA damage [34]. RIP1 may participate in NEMO sumoylation, which can regulate ataxia telangiectasia mutated (ATM), a nuclear double strand break-activated protein kinase which initiates IKK activation, resulting in activation of NF-κB via IκB degradation [35]. On the other hand, since JNK activation is independent of RIP1, we propose that the amplification loop between JNK and ROS may be a separate pathway other than RIP1.

Besides using MEFs as a model to investigate death signaling for parthanatos, we also observed the similar effects of MNNG-induced cell death in two cancer cell types. Although HeLa and HCT116 were more sensitive to MNNG-induced cell death at 50 μM, under the toxic dose of MNNG, significant ROS production, rapid PAR formation and JNK phosphorylaion can also be found in both cancer cells (Fig. 7). Thus, we may propose that no matter in normal or cancer cells, MNNG can initiate oxidative stress and PARP-1-dependent cell death.

In conclusion, our results for the first time reveal that ROS production is the key mediator and regulator of MNNG-induced cell death. We demonstrate biphasic ROS production after MNNG treatment in MEFs. NADPH oxidase may be the source of early-phase ROS production, while late-phase ROS production is from mitochondria and depends on RIP1. Moreover, the early phase of ROS production is the upstream signal for the intracellular calcium increase and contributes to DNA strand breaks, which together induce PARP-1 hyperactivation and depletion of ATP contents. The energy imbalance may eventually lead to mitochondrial dysfunction and ROS production. On the other hand, calcium-mediated JNK activation also contributes to late-phase ROS production. Overall, ROS production exerts amplification regulation on JNK activity and the intracellular calcium increase, and in turn contributes to cell death. We summarize the signaling cascades responsible for MNNG-induced cell death in Fig. 8. Since PARP-1-mediated cell death is involved in a variety of pathologic conditions, specific inhibitors targeting this pathway may provide future clinical benefits.

Acknowledgements

This work was supported by grants from the National Science Council, Taiwan (NSC98-2320-B-002-010-MY3 and NSC98-2320-B-400-001-MY3) and Frontier and Innovative Research of National Taiwan University (98R0335).

References

[1] Andrabi SA, Dawson TM, Dawson VL. Mitochondrial and nuclear cross talk in cell death: parthanatos. Ann N Y Acad Sci 2008;1147:233–41.
[2] Peralta-Leal A, Rodriguez-Vargas JM, Aguilar-Quesada R, Rodriguez MI, Linares JL, de Almodovar MR, et al. PARP inhibitors: new partners in the therapy of cancer and inflammatory diseases. Free Radic Biol Med 2009;47:13–26.
[3] Ha HC, Snyder SH. Poly(ADP-ribose) polymerase is a mediator of necrotic cell death by ATP depletion. Proc Natl Acad Sci USA 1999;96:13978–82.
[4] Yu SW, Wang H, Poitras MF, Coombs C, Bowers WJ, Federoff HJ, et al. Mediation of poly(ADP-ribose) polymerase-1-dependent cell death by apoptosis-inducing factor. Science 2002;297:259–63.
[5] Moubarak RS, Yuste VJ, Artus C, Bouharrour A, Greer PA, Menissier-de Murcia J, et al. Sequential activation of poly(ADP-ribose) polymerase 1, calpains, and Bax is essential in apoptosis-inducing factor-mediated programmed necrosis. Mol Cell Biol 2007;27:4844–62.

[6] Eliasson MJ, Sampei K, Mandir AS, Hurn PD, Traystman RJ, Bao J, et al. Poly(ADP-ribose) polymerase gene disruption renders mice resistant to cerebral ischemia. Nat Med 1997;3:1089–95.
[7] Virag L, Szabo C. The therapeutic potential of poly(ADP-ribose) polymerase inhibitors. Pharmacol Rev 2002;54:375–429.
[8] Kelliher MA, Grimm S, Ishida Y, Kuo F, Stanger BZ, Leder P. The death domain kinase RIP mediates the TNF-induced NF-kappaB signal. Immunity 1998;8:297–303.
[9] Meylan E, Tschopp J. The RIP kinases: crucial integrators of cellular stress. Trends Biochem Sci 2005;30:151–9.
[10] Holler N, Zaru R, Micheau O, Thome M, Attinger A, Valitutti S, et al. Fas triggers an alternative, caspase-8-independent cell death pathway using the kinase RIP as effector molecule. Nat Immunol 2000;1:489–95.
[11] Lin Y, Choksi S, Shen HM, Yang QF, Hur GM, Kim YS, et al. Tumor necrosis factor-induced nonapoptotic cell death requires receptor-interacting protein-mediated cellular reactive oxygen species accumulation. J Biol Chem 2004;279:10822–8.
[12] Chen TY, Chi KH, Wang JS, Chien CL, Lin WW. Reactive oxygen species are involved in FasL-induced caspase-independent cell death and inflammatory responses. Free Radic Biol Med 2009;46:643–55.
[13] Temkin V, Huang Q, Liu H, Osada H, Pope RM. Inhibition of ADP/ATP exchange in receptor-interacting protein-mediated necrosis. Mol Cell Biol 2006;26:2215–2225.
[14] Xu Y, Huang S, Liu ZG, Han J. Poly(ADP-ribose) polymerase-1 signaling to mitochondria in necrotic cell death requires RIP1/TRAF2-mediated JNK1 activation. J Biol Chem 2006;281:8788–95.
[15] Ermak G, Davies KJ. Calcium and oxidative stress: from cell signaling to cell death. Mol Immunol 2002;38:713–21.
[16] Guidarelli A, Fiorani M, Cantoni O. Calcium-dependent mitochondrial formation of species promoting strand scission of genomic DNA in U937 cells exposed to tert-butylhydroperoxide: the role of arachidonic acid. Free Radic Res 2000;33:477–87.
[17] Homburg S, Visochek L, Moran N, Dantzer F, Priel E, Asculai E, et al. A fast signal-induced activation of Poly(ADP-ribose) polymerase: a novel downstream target of phospholipase c. J Cell Biol 2000;150:293–307.
[18] Kun E, Kirsten E, Mendeleyev J, Ordahl CP. Regulation of the enzymatic catalysis of poly(ADP-ribose) polymerase by dsDNA, polyamines, Mg2+, Ca2+, histones H1 and H3, and ATP. Biochemistry 2004;43:210–6.
[19] Bentle MS, Reinicke KE, Bey EA, Spitz DR, Boothman DA. Calcium-dependent modulation of poly(ADP-ribose) polymerase-1 alters cellular metabolism and DNA repair. J Biol Chem 2006;281:33684–96.
[20] Haince JF, Rouleau M, Hendzel MJ, Masson JY, Poirier GG. Targeting poly(ADP-ribosyl)ation: a promising approach in cancer therapy. Trends Mol Med 2005;11:456–63.
[21] Yuste VJ, Moubarak RS, Delettre C, Bras M, Sancho P, Robert N, et al. Cysteine protease inhibition prevents mitochondrial apoptosis-inducing factor (AIF) release. Cell Death Differ 2005;12:1445–8.
[22] Kim YS, Morgan MJ, Choksi S, Liu ZG. TNF-induced activation of the Nox1 NADPH oxidase and its role in the induction of necrotic cell death. Mol Cell 2007;26:675–87.
[23] Yu SW, Andrabi SA, Wang H, Kim NS, Poirier GG, Dawson TM, et al. Apoptosis-inducing factor mediates poly(ADP-ribose) (PAR) polymer-induced cell death. Proc Natl Acad Sci USA 2006;103:18314–9.
[24] Zhang J, Dawson VL, Dawson TM, Snyder SH. Nitric oxide activation of poly(ADP-ribose) synthetase in neurotoxicity. Science 1994;263:687–9.
[25] Alano CC, Ying W, Swanson RA. Poly(ADP-ribose) polymerase-1-mediated cell death in astrocytes requires NAD + depletion and mitochondrial permeability transition. J Biol Chem 2004;279:18895–902.
[26] Virag L, Scott GS, Antal-Szalmas P, O'Connor M, Ohshima H, Szabo C. Requirement of intracellular calcium mobilization for peroxynitrite-induced poly(ADP-ribose) synthetase activation and cytotoxicity. Mol Pharmacol 1999;56:824–33.
[27] Byun JY, Kim MJ, Eum DY, Yoon CH, Seo WD, Park KH, et al. Reactive oxygen species-dependent activation of Bax and poly(ADP-ribose) polymerase-1 is required for mitochondrial cell death induced by triterpenoid pristimerin in human cervical cancer cells. Mol Pharmacol 2009;76:734–44.
[28] Huang Q, Wu YT, Tan HL, Ong CN, Shen HM. A novel function of poly(ADP-ribose) polymerase-1 in modulation of autophagy and necrosis under oxidative stress. Cell Death Differ 2009;16:264–77.
[29] Sakon S, Xue X, Takekawa M, Sasazuki T, Okazaki T, Kojima Y, et al. NF-kappaB inhibits TNF-induced accumulation of ROS that mediate prolonged MAPK activation and necrotic cell death. EMBO J 2003;22:3898–909.
[30] Ventura JJ, Cogswell P, Flavell RA, Baldwin Jr AS, Davis RJ. JNK potentiates TNF-stimulated necrosis by increasing the production of cytotoxic reactive oxygen species. Genes Dev 2004;18:2905–15.
[31] Kamata H, Honda S, Maeda S, Chang L, Hirata H, Karin M. Reactive oxygen species promote TNFalpha-induced death and sustained JNK activation by inhibiting MAP kinase phosphatases. Cell 2005;120:649–61.
[32] Temkin V, Karin M. From death receptor to reactive oxygen species and c-Jun N-terminal protein kinase: the receptor-interacting protein 1 odyssey. Immunol Rev 2007;220:8–21.
[33] Zhang DW, Shao J, Lin J, Zhang N, Lu BJ, Lin SC, et al. RIP3, an energy metabolism regulator that switches TNF-induced cell death from apoptosis to necrosis. Science 2009;325:332–6.
[34] Hur GM, Lewis J, Yang Q, Lin Y, Nakano H, Nedospasov S, et al. The death domain kinase RIP has an essential role in DNA damage-induced NF-kappa B activation. Genes Dev 2003;17:873–82.
[35] Mabb AM, Miyamoto S. SUMO and NF-kappaB ties. Cell Mol Life Sci 2007;64:1979–96.